Journal of Solid Mechanics Vol. 9, No. 3 (2017) pp. 568-586

Analysis of Rectangular Stiffened Plates Based on FSDT and Meshless Collocation Method

Sh. Hosseini , B. Soltani *

Faculty of Mechanical Engineering, University of Kashan, Kashan, Iran

Received 20 June 2017; accepted 18 August 2017

ABSTRACT

In this paper, bending analysis of concentric and eccentric beam stiffened square and rectangular plate using the meshless collocation method has been investigated. For detecting the governing equations of plate and beams, Mindlin plate theory and Timoshenko beam theory have been used, respectively, with the stiffness matrices of the plate and the beams obtained separately. The stiffness matrices of the plate and the beams were combined together using transformation equations to obtain a total stiffness matrix. Being independent of the mesh along with its simpler implementation process, compared to the other numerical methods, the meshless collocation method was used for analyzing the beam stiffened plate. In order to produce meshless shape functions, radial point interpolation method was used where moment matrix singularity problem of the polynomial interpolation method was fixed. Also, the Multiquadric radial basis function was used for point interpolations. Used to have solutions of increased accuracy and stability were polynomials with the radial basis functions. Several examples are presented to demonstrate the accuracy of the method used to analyze stiffened plates with the accuracy of the results showing acceptable accuracy that the employed method in analyzing concentric and eccentric beam stiffened square and rectangular plates.

Keywords: Beam stiffened plate; Concentric and eccentric stiffener; Meshless collocation method; Radial point interpolation.

1 INTRODUCTION

STIFFENED plates are widely used in different structures. High strength to weight ratios has made stiffened plates extensively used across such industrial applications as aerospace structures, road bridges, ship hulls, etc. Extensive researches have been done for the analysis of stiffened plates. The earliest models for the analysis of stiffened plates include grillage model [1] and orthotropic model [2]. Defining an equivalent thickness of stiffened plate, these models suffered from inadequate accuracy and efficiency. Therefore, new models are developed where the plate and stiffener are considered as separate structures with compatibility equations introduced to consider interactions between the plate and stiffeners ([3], [4] and [5]).

Different methods are used to analyze stiffened plates, such as Rayleigh-Ritz method [6], finite difference method [7], finite element method ([5], [8], and [9]), constrain method [4], finite strip method [10], and semi analytical finite difference method [11]. Wen et al. [12] used boundary element method to analyze stiffened plates. They used coupled boundary element formulation of shear deformable plate and two dimensional plane stress

*Corresponding author. Tel.: +98 912 809 2210; Fax: +98 361 591 2424.
E-mail address: bsoltani@kashanu.ac.ir (B.Soltani).

elasticity. It is necessary to use numerical methods instead of analytical approaches for such complex engineering structures as stiffened plates. Among other numerical methods, finite element method was taken into consideration due to its stability and efficiency. However, one of the main problems associated with this method is its reliance on mesh. Therefore, the idea of eliminating the meshes where the solutions are just dependent on the nodes, caused so-called meshless or mesh-free methods to emerge ([13] and [14]).

Peng et al. [3] investigated a rectangular stiffened plate based on element-free Galerkin method. Memar Ardestani et al. [15] studied an FGM stiffened plate based on reproducing kernel particle method. They studied the stability of RKPM for the analysis of stiffened plates.

One of the useful meshless methods is a meshless collocation method based on radial basis functions. With no background meshes required to be integrated into the meshless collocation method, it is truly meshless. Furthermore, it is simpler to formulate and implement compared to other meshless methods such as MLPG or EFG.

Recently, radial basis functions have enjoyed considerable success and research as a technique for interpolating data and functions. A radial basis function can be seen as a spline that depends on the Euclidian distance between distinct data centers also called nodal or collocation points. These functions resolve the singularity matrix in the polynomial point interpolation method. Also, Kronecker delta function properties imply that boundary conditions can be imposed with no special method required.

Kansa [16] introduced the concept of solving PDE's by an unsymmetric RBF collocation method based upon Multiquadrics interpolation functions.

Hardy [17] introduced multiquadrics for the analysis of scattered geographical data. In 1990s, Kansa [16] used multiquadrics to solve partial differential equations. The RBFs are insensitive to spatial dimensions, making the implementation of the method much easier than that of, e.g., finite elements. An important feature of RBF method is that it does not require a mesh. The only geometric property needed in a RBF approximation is the distance between the two points. Working with higher dimensional problems is not difficult as distances are easy to compute in spaces of any number of dimensions.

One of the main problems of collocation method is represented by its instability in the presence of derivative boundary conditions which may not only cause some instabilities in the solution of the problem, but may also lead to lower accuracy and even wrong results in some cases. There are, however, many ways to stabilize problems with derivative boundary conditions. Using Hermite-type collocation method, using fictitious points outside the problem domain, using regular grids within the problem domain along the derivative boundary, using meshless weak-strong form and the use of dense nodes near the derivative boundary are some of such ways, to name a few. Using dense nodes near the derivative boundary significantly increase the accuracy and stability of the results [13]. In this method, the more number of nodes are used across areas near the derivative boundary condition. Solid points in Fig. 1 show uniform node distribution in an arbitrary domain with the cross signs showing additional points introduced to increase the accuracy and stability of the results.

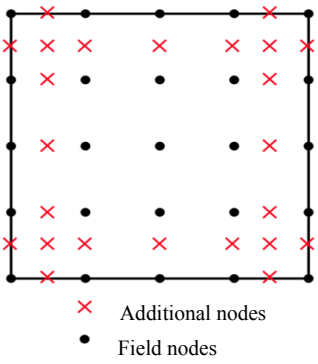

Fig.1
Using compact nodes in regions near to the derivative boundaries for increasing the stability and accuracy of the problem.

In this paper, the deflection of stiffened square and stiffened rectangular plates are studied using the collocation method based on radial basis functions. Point interpolations are performed via a multiquadric interpolation function. The boundary conditions are directly applied because of Kronecker delta function property of the shape functions. The interactions between the plate and stiffeners are imposed through the compatibility equations in which deflection of stiffeners is considered to be equal to that of the plate along the line of interactions.

2 MESHLESS COLLOCATION FORMULATION BASED ON RPIM

2.1 Radial point interpolation formulations

Radial basis approximation functions are meshless numerical schemes that can exploit accurate representations of the boundary, are easy to implement and can be spectrally accurate. In this paper, the formulation of a global unsymmetrical collocation RBF-based method to compute elliptic operators is presented.

Consider a linear elliptic partial differential operator L and a bounded region Ω in R^n within some boundary $\partial\Omega$. In a static problem, one may seek the computation of displacements u from a global system of equations.

$$Lu = f \qquad in\ \Omega \tag{1a}$$

$$L_B u = g \qquad in\ \partial\Omega \tag{1b}$$

where L and L_B are linear operators in the domain and on the boundary, respectively. The right-hand side of Eq. (1) represents the external forces applied in the internal domain and the boundary conditions applied along the perimeter of the problem, respectively (Fig. 2).

The radial basis function approximation of a function u is

$$u(x) = \sum_{i=1}^{n} R_i(x) a_i + \sum_{j=1}^{m} p_j(x) b_j = R(x)a + p(x)b \tag{2}$$

where $R_i(x)$ is a radial basis function, n is the number of RBFs, $p_j(x)$ is monomial in the space coordinates $x^T = [x, y]$, and m is the number of polynomial basis functions. When $m=0$, pure RBFs are used. Otherwise, the RBF is augmented with m polynomial basis functions. Coefficients a_i and b_j are constants. In the radial basis function $R_i(x)$, the variables are shape parameter c and the distance between the point of interest x and a node at x_i, that defined as:

$$r = |x - x_i| \qquad \text{for 1-}D\text{ problems} \tag{3a}$$

$$r = \sqrt{(x - x_i)^2 + (y - y_i)^2} \qquad \text{for 2-}D\text{ problems} \tag{3b}$$

The most common RBFs are:

Cubic: $\phi(r) = r^3$

Thin plate splines: $\phi(r) = r^2 \log(r)$

Gaussian: $\phi(r) = e^{-(cr)^2}$

Multiquadrics: $\phi(r) = \sqrt{c^2 + r^2}$

Inverse Multiquadrics: $\phi(r) = (c^2 + r^2)^{-1/2}$

where the Euclidian distance r is real and non-negative.

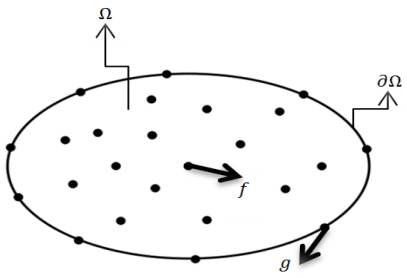

Fig.2
Node distribution on inner and boundary regions of global domain.

RPIM shape functions with pure RBFs usually cannot pass the standard patch tests. Adding polynomial terms up to the linear order can ensure the C^1 consistency that is needed to pass the standard patch test. In general, adding polynomials can always improve the accuracy of the results while reducing the sensitivity of the shape parameters, so that it will provide the user with much more freedom and a wider range of choosing shape parameters [19].

Coefficients a_i and b_j in Eq. (2) can be determined by enforcing Eq. (2) to be satisfied at all n nodes surrounding the point of interest x. This leads to n linear equations, one for each node. The matrix form of these equations can be expressed as follows

$$U_s = R_0 a + P_m b \tag{4a}$$

where the vector of function values U_s is

$$U_s = \{u_1, u_2, ..., u_n\}^T \tag{4b}$$

The moment matrix of RBFs is

$$R_0 = \begin{bmatrix} R_1(r_1) & R_2(r_1) & \cdots & R_n(r_1) \\ R_1(r_2) & R_2(r_2) & \cdots & R_n(r_2) \\ \vdots & \vdots & \ddots & \vdots \\ R_1(r_n) & R_2(r_n) & \cdots & R_n(r_n) \end{bmatrix}_{(n\times n)} \tag{4c}$$

The polynomial moment matrix is

$$P_m = \begin{bmatrix} 1 & x_1 & y_1 & \cdots & p_m(x_1) \\ 1 & x_2 & y_2 & \cdots & p_m(x_2) \\ \vdots & \vdots & \vdots & \ddots & \vdots \\ 1 & x_n & y_n & \cdots & p_m(x_n) \end{bmatrix}_{(m\times n)} \tag{4d}$$

The vector of coefficients of RBFs is

$$a = \{a_1, a_2, ..., a_n\}^T \tag{4e}$$

and the vector of coefficients for polynomial is

$$b = \{b_1, b_2, ..., b_m\}^T \tag{4f}$$

There are $n+m$ variables in Eq. (4a). The additional m equations can be added using the following m constraints conditions.

$$\sum_{i=1}^{n} p_j(x_i)a_i = P_m^T a = 0 \tag{5}$$

By combining Eq. (4a) and Eq. (5), yields the following set of equations in the matrix form

$$\tilde{U_s} = \begin{bmatrix} U_s \\ 0 \end{bmatrix} = \begin{bmatrix} R_0 & P_m^T \\ P_m & 0 \end{bmatrix} \begin{Bmatrix} a \\ b \end{Bmatrix} = G\, a_0 \tag{6a}$$

where

$$a_0 = \{a_1, a_2, ..., a_n, b_1, b_2, ..., b_m\}^T \tag{6b}$$

$$\tilde{U_s} = \{u_1, u_2, ..., u_n, 0, ..., 0\}^T \tag{6c}$$

By combining Eq. (6a) and Eq. (4a) and some simplification, RPIM shape functions can be expressed as:

$$\tilde{\Phi} = \begin{Bmatrix} R^T(x) & p^T(x) \end{Bmatrix} G^{-1} = \{\phi_1(x), \phi_2(x), ..., \phi_n(x), \phi_{n+1}(x), ..., \phi_{n+m}(x)\} \tag{7}$$

Finally, the RPIM shape functions corresponding to the nodal displacements vector $\Phi(x)$ are obtained as:

$$\Phi(x) = \{\phi_1(x), \phi_2(x), ..., \phi_n(x)\} \tag{8}$$

Eq. (2) can be rewritten as:

$$u(x) = \Phi^T(x) U_s = \sum_{i=1}^{n} \phi_i\, u_i \tag{9}$$

The derivatives of $u(x)$ are obtained as:

$$u_{,l}(x) = \Phi_{,l}(x) U_s \tag{10}$$

where l denotes either the coordinates x or y.

The choice of shape parameter directly influences the accuracy of results. Hardy [17] suggests the use of $c = 0.815d$, where $d = \frac{1}{N}\sum_{i=1}^{N} d_i$, and d_i is the distance from the data point x_i to its nearest neighbor. Franke [18], on the other hand, recommends $c = \frac{1.25D}{\sqrt{N}}$, where D is the diameter of the smallest circle containing all data points. Fasshauer [19] argues the use of $c = \frac{2}{\sqrt{N_a}}$, where N_a is the number of collocation points in either x- or y- direction. Ferreira et al. [20] suggest $c = \frac{1}{\sqrt{N_a}}$ for plates with $\frac{a}{h} \le 15$.

In this paper, we used the Multiquadric radial basis function to interpolate scattered points. The shape parameter has been chosen to be $c = \frac{1}{\sqrt{N_a}}$ for plates with unit length of side and $c = \frac{\alpha D}{\sqrt{N}}$ for plates of non-identical lengths of the sides, where α is a user defined parameter that is different in different problems.

2.2 Stiffness matrix

The global system of equations mentioned in Eq. (1). By substituting Eq. (9) into Eq. (1), results

$$L(\Phi U_s) = f \tag{11a}$$

$$L_B(\Phi U_s) = g \tag{11b}$$

By putting Eq. (11) in a matrix form, the global stiffness matrix is formed

$$K_{N\times N}\, U_{N\times 1} = F_{N\times 1} \tag{12a}$$

where stiffness matrix, K, is

$$K = \left[L(\Phi(\mathrm{X}_1)),...,L(\Phi(\mathrm{X}_{NI})),L_B(\Phi(\mathrm{X}_{NI+1})),...,L_B(\Phi(\mathrm{X}_{NB}))\right]^T \tag{12b}$$

Nodal values vector, U, is

$$U = \left[u_1, u_2, ..., u_{NI}, u_{NI+1}, ..., u_{NB}\right]^T \tag{12c}$$

and the global source vector F consists of

$$F = \left[f(X_1), f(X_2), ..., f(X_{NI}), g(X_{NI+1}), ..., g(X_{NB})\right]^T \tag{12d}$$

The Eq. (12a) can be solved by using common methods for solving the system of equation.

3 COMPATIBILITY EQUATIONS

Transformation equations were used to combine the stiffness matrix of plate and beams. The stiffener is considered to be attached to the lower side of the plate. The meshless model of a stiffened plate is shown in Fig. 2. Some of the nodes are subscriber between plate and stiffener, so that the compatibility conditions of the stiffened plate can be written as follows:

$$\left[w^p\right]_{z=-h_p/2} = \left[w^s\right]_{z=-h_s/2} \tag{13a}$$

$$\left[\theta_x^p\right]_{z=-h_p/2} = \left[\theta_x^s\right]_{z=-h_s/2} \tag{13b}$$

$$\left[\theta_y^p\right]_{z=-h_p/2} = \left[\theta_y^s\right]_{z=-h_s/2} \tag{13c}$$

where h_p is the thickness of the plate and h_s is the depth of the x-stiffener. Subscript s and p are generic notations which refer to x- or y- stiffener and plate, respectively.

By using RPIM shape functions, Eq. (13) can be reformulated as:

$$\sum_{j=1}^{n_p}\begin{bmatrix}\phi_j^p(X_i) & 0 & 0\\ 0 & \phi_j^p(X_i) & 0\\ 0 & 0 & \phi_j^p(X_i)\end{bmatrix}\begin{bmatrix}w_j^p\\ \theta_{xj}^p\\ \theta_{yj}^p\end{bmatrix}=\sum_{j=1}^{n_s}\begin{bmatrix}\phi_j^s(X_i) & 0 & 0\\ 0 & \phi_j^s(X_i) & 0\\ 0 & 0 & \phi_j^s(X_i)\end{bmatrix}\begin{bmatrix}w_j^s\\ \theta_{xj}^s\\ \theta_{yj}^s\end{bmatrix},\quad (i=1,...,n_s) \tag{14}$$

where n_p and n_s are the number of nodes on the plate domain and stiffener domain, respectively. The matrix form of Eq. (14) expressed as:

$$T^p\delta^p = T^s\delta^s \tag{15a}$$

where T^p, T^s, δ^p and δ^s defined as follows

$$T^p=\begin{bmatrix}\phi_1^p(X_1) & 0 & 0 & \dots & \phi_{n_p}^p(X_1) & 0 & 0\\ 0 & \phi_1^p(X_1) & 0 & \dots & 0 & \phi_{n_p}^p(X_1) & 0\\ 0 & 0 & \phi_1^p(X_1) & \dots & 0 & 0 & \phi_{n_p}^p(X_1)\\ \vdots & \vdots & \vdots & \ddots & \vdots & \vdots & \vdots\\ \phi_1^p(X_{n_s}) & 0 & 0 & \dots & \phi_{n_p}^p(X_{n_s}) & 0 & 0\\ 0 & \phi_1^p(X_{n_s}) & 0 & \dots & 0 & \phi_{n_p}^p(X_{n_s}) & 0\\ 0 & 0 & \phi_1^p(X_{n_s}) & \dots & 0 & 0 & \phi_{n_p}^p(X_{n_s})\end{bmatrix}_{(3n_s\times 3n_p)},\quad \delta^p=\begin{bmatrix}w_1^p\\ \theta_{x1}^p\\ \theta_{y1}^p\\ \vdots\\ w_{n_p}^p\\ \theta_{xn_p}^p\\ \theta_{yn_p}^p\end{bmatrix}_{(3n_p\times 1)} \tag{15b}$$

$$T^s=\begin{bmatrix}\phi_1^s(X_1) & 0 & 0 & \dots & \phi_{n_s}^s(X_1) & 0 & 0\\ 0 & \phi_1^s(X_1) & 0 & \dots & 0 & \phi_{n_s}^s(X_1) & 0\\ 0 & 0 & \phi_1^s(X_1) & \dots & 0 & 0 & \phi_{n_s}^s(X_1)\\ \vdots & \vdots & \vdots & \ddots & \vdots & \vdots & \vdots\\ \phi_1^s(X_{n_s}) & 0 & 0 & \dots & \phi_{n_p}^s(X_{n_s}) & 0 & 0\\ 0 & \phi_1^s(X_{n_s}) & 0 & \dots & 0 & \phi_{n_p}^s(X_{n_s}) & 0\\ 0 & 0 & \phi_1^s(X_{n_s}) & \dots & 0 & 0 & \phi_{n_p}^s(X_{n_s})\end{bmatrix}_{(3n_s\times 3n_s)},\quad \delta^s=\begin{bmatrix}w_1^s\\ \theta_{x1}^s\\ \theta_{y1}^s\\ \vdots\\ w_{n_s}^s\\ \theta_{xn_s}^s\\ \theta_{yn_s}^s\end{bmatrix}_{(3n_s\times 1)} \tag{15c}$$

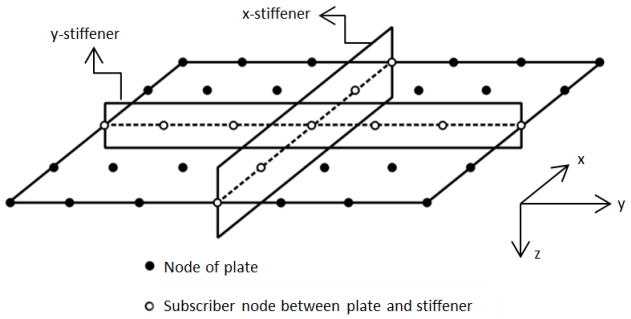

Fig.3
Node distribution in stiffened plate.

In general, the transformation equations can be obtained as:

$$\delta^{s} = (T^{s})^{-1} T^{p} \delta^{p} \tag{16}$$

For *x*- and *y*-stiffener, Eq. (16) can be reformulated as:

$$\delta^{sx} = (T^{sx})^{-1} I^{sx} T^{p} \delta^{p} \tag{17a}$$

$$\delta^{sy} = (T^{sy})^{-1} I^{sy} T^{p} \delta^{p} \tag{17b}$$

where

$$I^{sx} = \begin{bmatrix} 1 & & & & & & \\ & 1 & & & 0 & & \\ & & 0 & & & & \\ & & & \ddots & & & \\ & & & & 1 & & \\ & & 0 & & & 1 & \\ & & & & & & 0 \end{bmatrix}_{(3n_{sx} \times 3n_{sx})}, \quad I^{sy} = \begin{bmatrix} 1 & & & & & & \\ & 0 & & & 0 & & \\ & & 1 & & & & \\ & & & \ddots & & & \\ & & & & 1 & & \\ & & 0 & & & 0 & \\ & & & & & & 1 \end{bmatrix}_{(3n_{sy} \times 3n_{sy})} \tag{17c}$$

where n_{sx} and n_{sy} are the number of nodes on *x*- and *y*-stiffener, respectively. Finally, by using the transformation equations for beam stiffened plate, total stiffness matrix defined as:

$$K = K_{p} + \sum_{i=1}^{N_{sx}} ((T_{i}^{sx})^{-1} I^{sx} T^{p})^{T} K_{sx}^{i} ((T_{i}^{sx})^{-1} I^{sx} T^{p}) + \sum_{i=1}^{N_{sy}} ((T_{i}^{sy})^{-1} I^{sy} T^{p})^{T} K_{sy}^{i} ((T_{i}^{sy})^{-1} I^{sy} T^{p}) \tag{18}$$

where N_{sx} and N_{sy} denote the number of stiffeners in *x*- and *y*-directions, respectively.

4 GOVERNING EQUATIONS OF STIFFENED PLATE

4.1 Governing equations of Timoshenko beam

Displacement field for Timoshenko beam is

$$u = u_{0} + z\,\theta^{sx} \tag{19a}$$

$$w = w_{0} \tag{19b}$$

In-plane displacement of the beam (u_0) is very small and it can be neglected. The strain fields defined as:

$$\varepsilon_{x} = \frac{\partial u}{\partial x} = z\,\frac{\partial \theta^{sx}}{\partial x} \tag{20a}$$

$$\gamma_{xz} = \frac{\partial w}{\partial x} + \frac{\partial u}{\partial z} = \frac{\partial w_{0}}{\partial x} + \theta^{sx} \tag{20b}$$

The virtual strain energy with shear strain virtual energy is

$$\delta U = \int_0^L \int_A (\sigma_{xx}\, z\, \delta\theta^{sx}_{,x} + \tau_{xz}\, [\delta w_{0,x} + \delta\theta^{sx}])dA\, dx = \int_0^L [M_{xx}\, \delta\theta^{sx}_{,xx} + Q_x\, (\delta\theta^{sx} + \delta w_{0,x}]dx \tag{21}$$

where σ_{xx}, τ_{xz}, M_{xx} and Q_x are normal stress, shear stress, bending moment and shear force, respectively and defined as:

$$M_{xx} = \int_A z\, \sigma_{xx}\, dA \tag{22a}$$

$$Q_x = \int_A \tau_{xz}\, dA \tag{22b}$$

Virtual potential energy from $\hat{q}$ load, is

$$\delta V = -\int_0^L \hat{q}(x)\, \delta w_0\, dx \tag{23}$$

By substuting virtual strain energy and virtual potential energy in virtual work principle and separating the factors of δw_0 and $\delta\theta^{sx}$, equilibrium equations obtained as:

$$-M_{xx,x} + Q_x = 0 \tag{24a}$$

$$-Q_{x,x} = \hat{q} \tag{24b}$$

By combining bending moment, shear force and equilibrium equations, governing equations of the *x*-stiffener obtained as:

$$A_{xz}\, (\theta^{sx}_{,x} + w_{0,xx}) = \hat{q}(x) \tag{25a}$$

$$D_{xx}\, \theta^{sx}_{,xx} - K_s A_{xz}\, (\theta^{sx} + w_{0,x}) = 0 \tag{25b}$$

where K_s is shear correction factor and A_{xz} and D_{xx} defined as:

$$A_{xz} = \int_A G_{xz}\, dA = G_{xz}\, A \tag{26a}$$

$$D_{xx} = \int_A E\, z^2\, dA = E\, I_{yy} \tag{26b}$$

Boundary conditions for Timoshenko beam are

$$w_0 = 0 \;,\; \theta^{sx} = 0 \qquad \text{Clamped} \tag{27a}$$

$$w_0 = 0 \;,\; M_{xx} = 0 \qquad \text{Simply Supported} \tag{27b}$$

$$Q_x = 0 \;,\; M_{xx} = 0 \qquad \text{Free} \tag{27c}$$

Similarly, governing equations of *y*-stiffener are

$$A_{yz}\, (\theta^{sy}_{,y} + w_{0,yy}) = \hat{q}(y) \tag{28a}$$

$$D_{yy}\,\theta^{sy}_{,yy} - K_s A_{yz}\,(\theta^{sy} + w_{0,y}) = 0 \tag{28b}$$

where A_{yz} and D_{yy} are

$$A_{yz} = \int_A G_{yz}\, dA = G_{yz}\, A \tag{29a}$$

$$D_{yy} = \int_A E\, z^2\, dA = E\, I_{xx} \tag{29b}$$

4.2 Governing equations of Mindlin plate

Displacement field for Mindlin plate is

$$u = u_0 + z\,\theta^{px} \tag{30a}$$

$$v = v_0 + z\,\theta^{py} \tag{30b}$$

$$w = w_0 \tag{30c}$$

where θ^{px} and θ^{py} denote the rotation around *y*- and *x*- axis, respectively. In-plane displacements (u_0 and v_0) are very small and negligible.

Linear strain components are

$$\varepsilon_{xx} = \frac{\partial u}{\partial x} = z\,\frac{\partial \theta^{px}}{\partial x} \tag{31a}$$

$$\varepsilon_{yy} = \frac{\partial v}{\partial y} = z\,\frac{\partial \theta^{py}}{\partial y} \tag{31b}$$

$$\gamma_{xy} = \frac{\partial u}{\partial y} + \frac{\partial v}{\partial x} = z\,(\frac{\partial \theta^{px}}{\partial y} + \frac{\partial \theta^{py}}{\partial x}) \tag{31c}$$

$$\gamma_{xz} = \frac{\partial w}{\partial x} + \frac{\partial u}{\partial z} = \frac{\partial w_0}{\partial x} + \theta^{px} \tag{31d}$$

$$\gamma_{yz} = \frac{\partial w}{\partial y} + \frac{\partial v}{\partial z} = \frac{\partial w_0}{\partial y} + \theta^{py} \tag{31e}$$

Equilibrium equations of Mindlin plate obtained from virtual work principle ($\delta W = \delta U + \delta V = 0$). Virtual strain energy and virtual potential energy are

$$\delta U = \int_A \left[\int_{-h/2}^{h/2} (\sigma_{xx}\,\delta\varepsilon_{xx} + \sigma_{yy}\,\delta\varepsilon_{yy} + \sigma_{xy}\,\delta\gamma_{xy} + \sigma_{xz}\,\delta\gamma_{xz} + \sigma_{yz}\,\delta\gamma_{yz})\, dz \right] dx\, dy \tag{32a}$$

$$\delta V = -\int_A q(x,y)\,\delta w_0\,dx\,dy \tag{32b}$$

Finally the equilibrium equations obtained by separating the coefficients of $\delta w_0, \delta\theta^{px}$ and $\delta\theta^{py}$.

$$Q_{x,x} + Q_{y,y} = q(x,y) \tag{33a}$$

$$M_{xx,x} + M_{xy,y} - Q_x = 0 \tag{33b}$$

$$M_{yy,y} + M_{xy,x} - Q_y = 0 \tag{33c}$$

where the resultant moments and forces are

$$[M_{xx}, M_{yy}, M_{xy}] = \int_{-h/2}^{h/2} [\sigma_{xx}, \sigma_{yy}, \sigma_{xy}]\, z\, dz \tag{34a}$$

$$[Q_x, Q_y] = K_s \int_{-h/2}^{h/2} [\sigma_{xz}, \sigma_{yz}]\, dz \tag{34b}$$

Governing equations of Mindlin plate in terms of displacements, obtained as:

$$\frac{K_s Eh}{2(1+\nu)}(w_{0,xx} + w_{0,yy} + \theta^{px}_{,x} + \theta^{py}_{,y}) = q(x,y) \tag{35a}$$

$$\frac{D(1-\nu)}{2}(\theta^{px}_{,xx} + \theta^{px}_{,yy}) + \frac{D(1+\nu)}{2}(\theta^{px}_{,xx} + \theta^{py}_{,yx}) - \frac{K_s Eh}{2(1+\nu)}(w_{0,x} + \theta^{px}) = 0 \tag{35b}$$

$$\frac{D(1-\nu)}{2}(\theta^{py}_{,xx} + \theta^{py}_{,yy}) + \frac{D(1+\nu)}{2}(\theta^{px}_{,yx} + \theta^{py}_{,yy}) - \frac{K_s Eh}{2(1+\nu)}(w_{0,y} + \theta^{py}) = 0 \tag{35c}$$

where $D = \dfrac{E\,h^3}{12(1-\nu^2)}$, is bending stiffness.

5 NUMERICAL RESULTS AND DISCUSSION

In this section several numerical examples are given to demonstrate the ability of the meshless RPIM collocation method in the analysis of beam stiffened plate.

5.1 Simply supported square plate with one rectangular stiffener

In the first study a simply supported square plate with one stiffener of rectangular cross section along *x*-direction (*y*=0.5 *in.*) is considered as shown in Fig. 4. A uniformly distributed load of 1.0 *psi* is applied to the top surface of the plate. Elastic properties of the plate and stiffener are assumed to be $E = 1.7e7\ psi$ and $\nu = 0.3$.

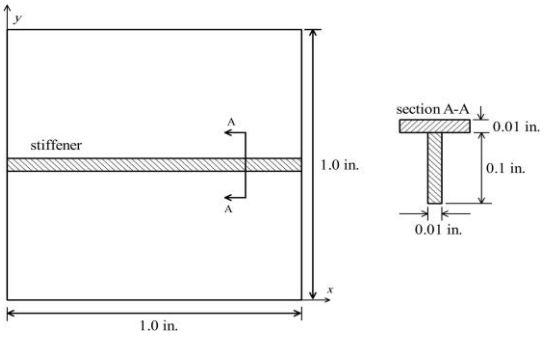

Fig.4
Square plate with one stiffener along y=0.5 *in*.

This example has been solved by McBean [8] and Rossow [4] using the FEM and become a benchmark problem in the field of stiffened plates. 15×15 nodes are considered to discretize the plate and 15 nodes are used for x-stiffener. The considered shape parameters are $c_p = \frac{1}{\sqrt{15}}$ for plate and $c_s = 7.7e(-3)$ and $c_s = 5.8e(-3)$ for concentric and eccentric stiffeners, respectively. The analysis results of concentric and eccentric stiffened plates are shown in Figs. 5 and 6, respectively, where they are also compared to the results of Peng et al. [3], Rossow [4], McBean [8] and Memar Ardestani et al. [15]. Also, Table 1. reports the results of the center deflection of the stiffened plate compared to those given by Peng et al. [3], Rossow [4], McBean [8] and Memar Ardestani et al. [15].

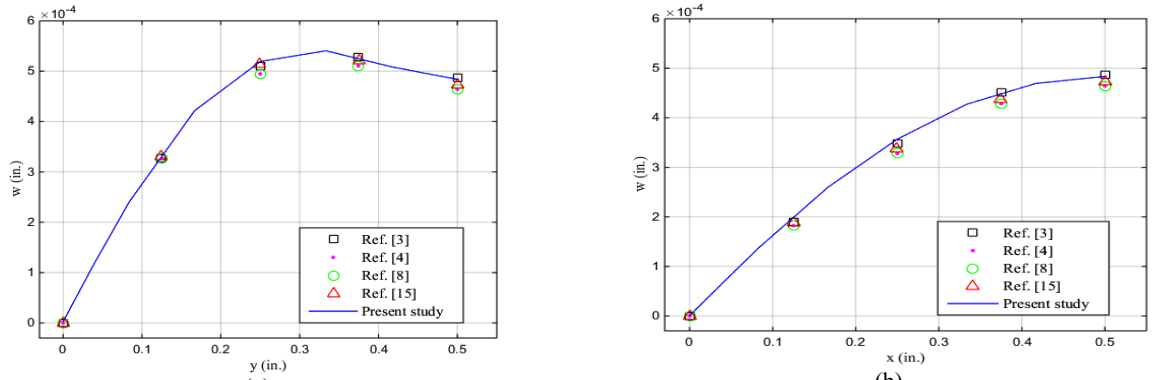

(a) (b)

Fig.5
Deflection of concentrically square stiffened plate with simply supported boundary condition along (a)x=0.5 *in.* and (b) y=0.5*in.*

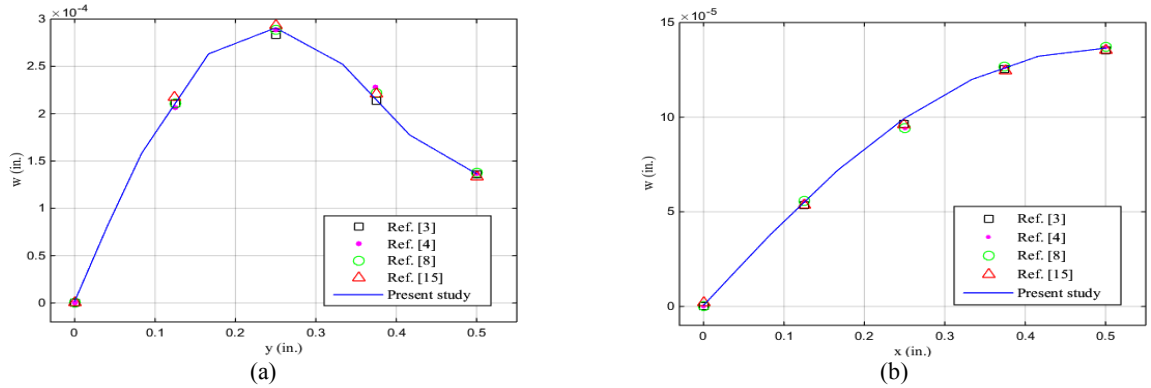

(a) (b)

Fig.6
Deflection of eccentrically square stiffened plate with simply supported boundary condition along (a) x=0.5 *in.* and (b) y=0.5*in.*

Table1
Center deflection of square stiffened plate for concentric and eccentric configurations.

Ref.	*Concentric*	*RD*(%)*	*Eccentric*	*RD (%)*
Peng et al [3]	4.8425e-4	0.1280	1.3516e-4	0.9692
Rossow [4]	4.556e-4	6.1523	1.367e-4	0.1682
McBean [8]	4.557e-4	6.1290	1.367e-4	0.1682
Memar Ardestani et al. [15]	4.7150e-4	2.5726	1.3801e-4	1.1159
Present	4.8363e-4		1.3647e-4	

**Relative Difference*

Due to the results of the Table 1, maximum and minimum relative differences are 6.1523%, with that result of Rossow [4] and 0.1280% with that result of Peng et al. [3], respectively. The nearest references from the aspect of assumptions in the formulation of the problem and numerical method are Ref. [3] and Ref. [15]. The relative differences between the present results and these references are in the acceptable range. Also, due to Figs. 5 and 6, the results for the other nodes have acceptably accurate compared to the references.

Fig. 7 shows corresponding deflection contours to the stiffened plate by one concentric rectangular beam.

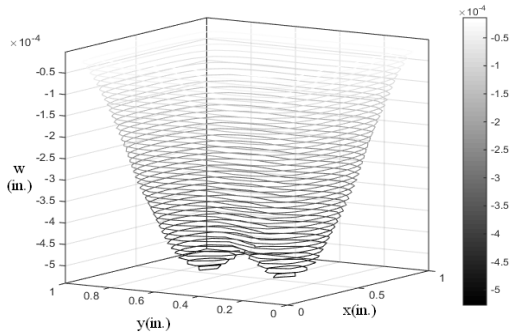

Fig.7
Deflection contour of stiffened plate by one concentric rectangular beam.

5.2 Simply supported and clamped square plate with one rectangular stiffener

This example is the same as before, except that it has changed boundary conditions. Edges along *y* and *x*-axis considered to be clamped and simply supported, respectively. Shape parameters are considered same as before. Fig. 8 shows the dimensions of the plate and stiffener and the position of boundary conditions.

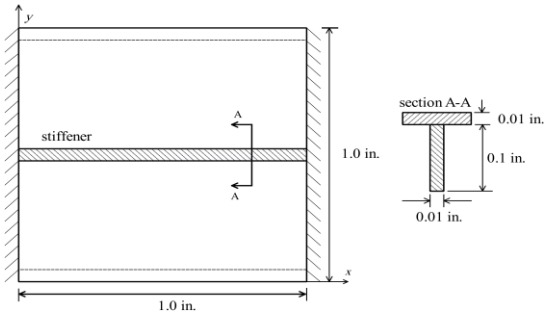

Fig.8
Square plate with one stiffener along *y*=0.5 *in*. and various boundary condition.

The results are compared to those results of Abaqus analysis. The number of elements has been considered as 14×14 (15×15 *nodes*). The element types of the plate and stiffener are *S4R* and *B31,* respectively. The results of eccentric stiffened plates with simply supported and clamped edges are shown in Fig. 9, where they are also compared to those results of Abaqus. By increasing the number of nodes in the areas close to the clamped edges, the accuracy of the results will be increased. The results of Fig. 9 show that the *MCM* has an acceptably accurate in various boundary conditions.

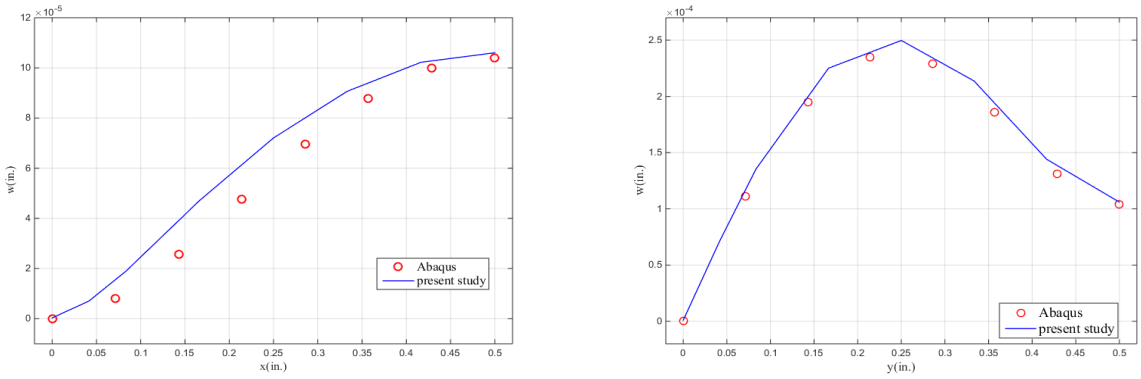

(a) (b)

Fig.9
Deflection of eccentrically square stiffened plate with simply supported and clamped boundary condition along (a) *y*=0.5 *in*. and (b) *x*=0.5 *in*.

5.3 Simply supported square plate with one I-shape stiffener

This problem is similar to the problem in Section 5.1, except for the fact that cross section of beam is *I*-shape and the beam is concentric with the plate. Also, the thickness of the plate was considered to be 0.1 *in.* Fig. 10 shows the dimensions of the plate and the stiffener.

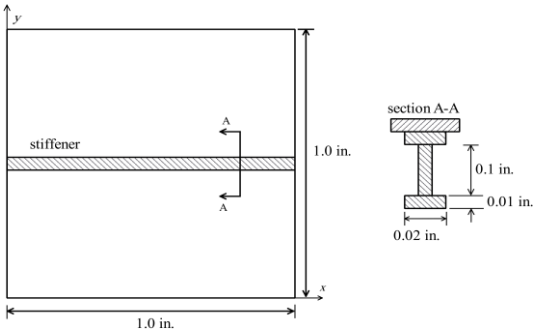

Fig.10
Square plate with one *I*-shape stiffener along *y*=0.5 *in.*

For solving this problem, 15×15 *nodes* are considered and shape parameter for plate, $c_p = \frac{1}{\sqrt{15}}$, and for stiffener, $c_s = 7.7e(-3)$, have been intended. The results are compared to those results of Peng et al. [3] and are shown in Fig. 11. Due to the Fig. 11, bending of the stiffened plate is symmetric and the maximum deflection is happening in the center of the plate, because the thickness of the plate is more than that of the previous problem; therefore the stiffness matrix is increasing or plate gets harder.

5.4 Simply supported square plate with one T-shape stiffener

In this problem, elastic properties of the plate and the stiffener are same as those in the problem presented in Section 5.1, except for the fact that the beam is considered to be concentric, with a *T*-shape cross section.

For the sake of solving this problem, 15×15 *nodes* were considered and the shape parameters were chosen to be $c_p = \frac{1}{\sqrt{15}}$ for the plate and $c_s = 7.7e(-3)$ for the stiffener.

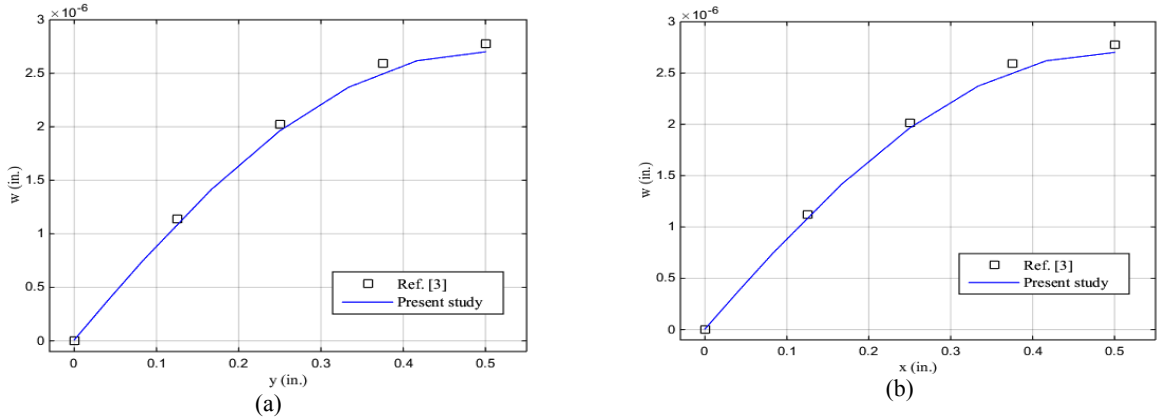

Fig.11
Deflection of concentrically square I-shape stiffened plate with simply supported boundary condition along (a) *x*=0.5 *in.* and (b) *y*=0.5 *in.*

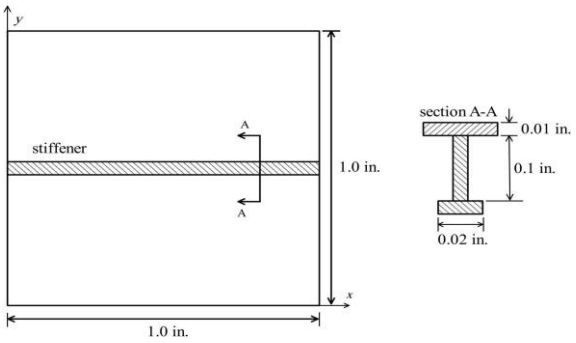

Fig.12
Square plate with one T-shape stiffener along *y*=0.5 *in.*

Fig. 13 compares the numerical results of the present paper to those of Peng et al. [3]. Similar to the previous example, bending of the stiffened plate is symmetric and the maximum deflection is happening in the center of the plate. Also, due to Fig. 13 the results are corresponding to those of Peng et al. [3].

5.5 Simply supported rectangular plate centrally stiffened by two stiffeners

A simply supported rectangular plate centrally stiffened by two stiffeners is subjected to a uniformly distributed load of 10.0 *psi*. Dimensions of the plate and the stiffeners are shown in Fig. 14. The plate and the stiffeners are made of the same material, with the elastic modulus of $E = 3e7\,psi$ and Poisson ratio of $\nu = 0.3$.

Concentric and eccentric stiffeners were considered. This problem has been solved by Rossow et al. [4] (using FEM) and Chang [21] (using FEM and analytical solution). Because in this case, the distances between the nodes are identical, 19×11 *nodes* were considered to solve this problem. The shape parameters for the plate, *x*-stiffener, and *y*-stiffener were taken as $c_p = \frac{1.5D}{\sqrt{N}}, c_{sx} = 1.4$ and $c_{sy} = 1.15$, respectively.

The deflections of concentric and eccentric stiffened plates at *x* = 7.5 *in.* and *x* = 15 *in.* are shown in Figs. 15 and 16, respectively. The deflection contours of the concentric stiffened plate by the two concentrically stiffeners are shown in Fig. 17. As can be seen in Figs. 15 to 17, maximum deflection is not happening in the center of the plate and the area of the plate is divided into four parts.

Fig. 18 demonstrates the corresponding moment diagram for this problem at *y* = 15 *in.* for the concentric and eccentric stiffeners.

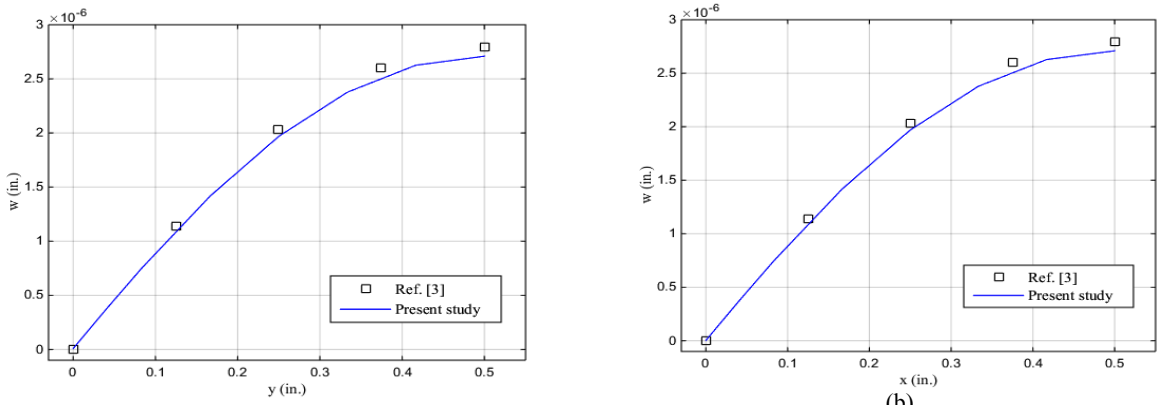

Fig.13
Deflection of concentrically square T-shape stiffened plate with simply supported boundary condition along (a) x=0.5 *in.* and (b) y=0.5 *in.*

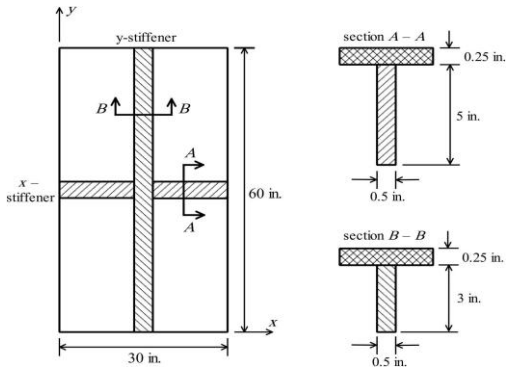

Fig.14
Simply supported rectangular plate centrally stiffened by two stiffeners.

Minor differences in the deflection of the rectangular stiffened plate were observed between the proposed method in the present paper and references, due to different theoretical bases and assumptions. The main target is to determine the deflection of the nodes on the boundaries and on the stiffeners. As can be seen in Figs. 15 and 16, zero deflection is determined at boundaries with the deflections of the nodes on the stiffeners enjoying acceptable accuracy. Similar to the previous case, differences in moments stem from differences in the assumptions and solution method.

5.5 Simply supported square plate orthogonally stiffened by equidistant stiffeners

A simply supported square plate of side length 2.0m and thickness 0.02m is orthogonally stiffened with equally spaced stiffeners of rectangular section (depth 0.1m, width 0.01m). The plate is subjected to a uniformly distributed load of q=6 t/m^2. The numbers of the stiffeners are 14+14, 12+12, 10+10, 8+8, 6+6 and 4+4. A square plate orthogonally stiffened by 4+4 stiffeners has been shown in Fig. 19.

The plates and stiffeners are made of the same material, with the elastic modulus of E=2.1e7 t/m^2 and the Poisson ratio of ν=0.3. The numbers of nodes for each problem have been chosen to be $(N_s+4)\times(N_s+4)$ (with N_s denoting the number of stiffeners in x- or y-direction), except for the 4+4 stiffeners, as the problem fails to provide stability with (8×8) *nodes* at which node configuration the results render inaccurate. Consequently, the number of nodes for 4+4 stiffeners was chosen to be (13×13).

The shape parameter was taken as $c_p = \dfrac{2D}{\sqrt{N}}$ for the plate; however, regarding various numbers of nodes, the shape parameter was chosen to be $c_s = 1.3 \sim 12.5\times10^{-3}$ for the stiffeners.

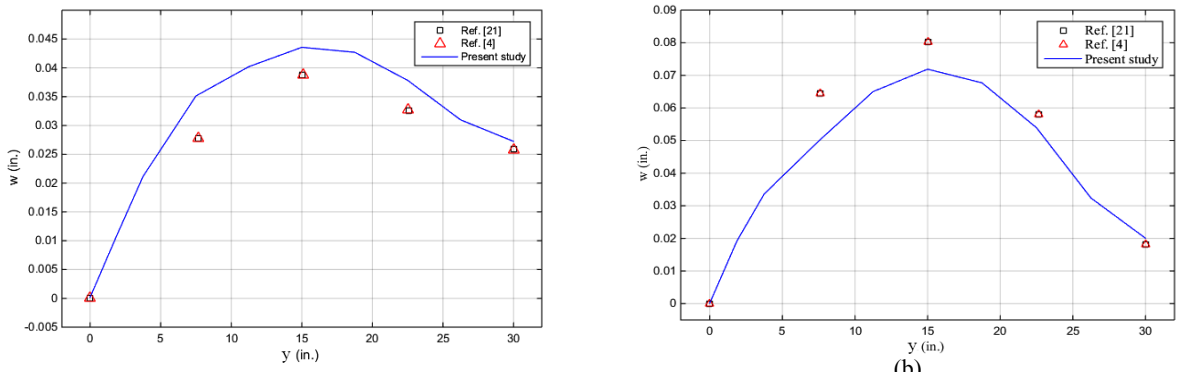

Fig.15
Deflection of concentrically rectangular stiffened plate with simply supported boundary condition along (a) x=7.5 *in.* and (b) y=7.5 *in.*

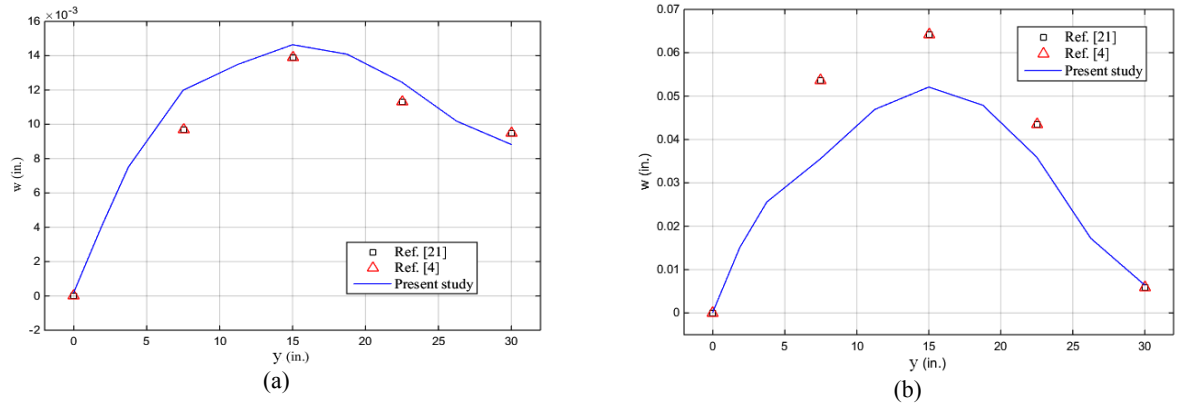

Fig.16
Deflection of eccentrically rectangular stiffened plate with simply supported boundary condition along (a) x=7.5 *in.* and (b) y=7.5 *in.*

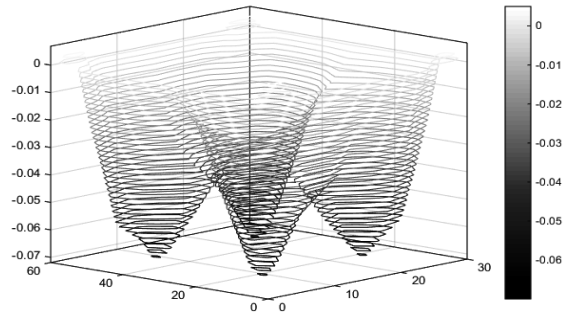

Fig.17
Deflection contour of the concentric stiffened plate by two beams in x- and y- direction.

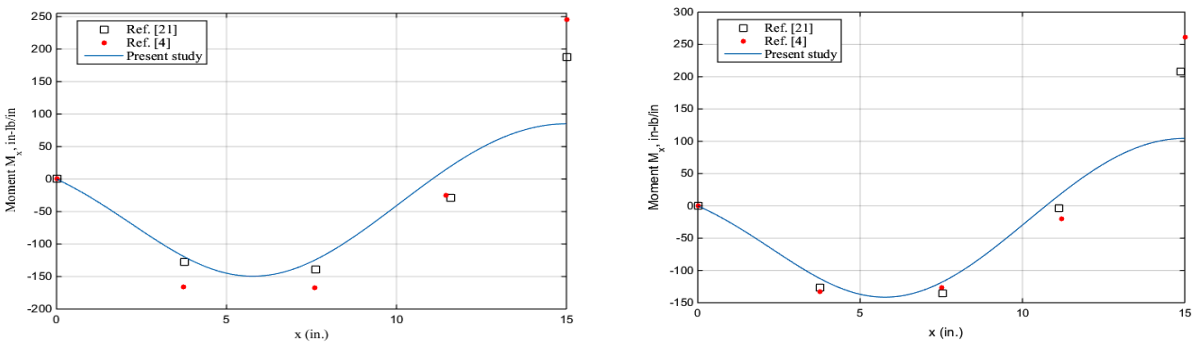

Fig.18
Diagram of moment of rectangular stiffened by two stiffeners in y=15 *in.* for (a) concentric and (b) eccentric stiffener.

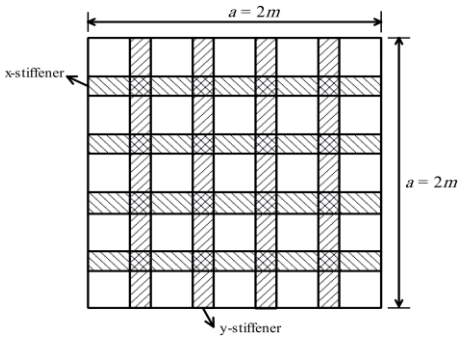

Fig.19
A square plate orthogonally stiffened by four stiffener in each direction.

Table 2. reports the results of the maximum deflection of the stiffened plate compared to those given by Deb and Booton [22], Biswal and Ghosh [23], Sadek and Tawfik [5] and Peng et al. [3]. The table demonstrates the maximum deflection reduction by increasing the number of stiffeners. The differences between the references come from different assumptions and formulations used to solve the problems. In terms of the assumptions taken, Ref. [3] represents the closest reference to the present research. The minimum and maximum relative difference between the present results and those results of reference [3] are 0.2490% and 4.8793%, respectively where, they are in an acceptably range.

Table 2
Maximum deflection of stiffened plate by equal distance beams in two directions ($m\times10^3$).

Number of stiffeners in two directions	FEM Ref. [22]	Orthotropic Ref. [22]	Ref. [23]	Ref. [5]	Ref. [3]	Present results
14+14	1.288	1.363	1.1999	1.2414	1.1388	1.1249
12+12	1.452	1.553	1.3726	1.4025	1.2849	1.2881
10+10	1.683	1.814	1.5804	1.6191	1.5078	1.4874
8+8	2.010	2.195	2.0189	1.9256	1.8273	1.8018
6+6	2.479	2.811	2.4909	2.3933	2.3261	2.3176
4+4	3.365	3.391	3.2824	3.1967	3.2156	3.0587

6 CONCLUSIONS

In this study, a meshless collocation method was used to analyze a simply supported rectangular stiffened plate based on FSDT. Radial point interpolation method based on multiquadric function was used for producing shape functions. Two cases of concentric and eccentric stiffeners were considered. The total potential energy principle was used to derive governing equations of the stiffened plate.

Same as the references, the results show that the maximum deflection of thinner stiffened plates is not happening in the center of the plate and for thicker stiffened plates, it happens in the center of the plate. Unlike FEM, using mesh-free RPIM method, no mesh generation is needed with the positions of the stiffeners being arbitrary. Also, mesh-free RPIM method is less complex and truly meshless as it does not need any integration. Therefore, the CPU-run-time of this method is significantly less than the other methods. Due to eliminating of the integration, the error of the numerical integration is removed and the accuracy of the results is increased. Enjoying acceptable accuracy, the results proved this method to be an efficient approach for stiffened plates.

REFERENCES

[1] Kendrick S., 1995, The analysis of a flat plated grillage, *European Shipbuilding* **5**: 4-10.

[2] Schade H., 1940, The orthogonally stiffened plate under uniform lateral load, *Journal of Applied Mechanics ASME* **62**: 143-146.

[3] Peng L., Kitipornchai S., Liew K., 2005, Analysis of rectangular stiffened plates under uniform lateral load based on FSDT and element-free Galerkin method, *International Journal of Mechanical Sciences* **47**(2): 251-276.

[4] Rossow M., Ibrahimkhail A., 1978, Constraint method analysis of stiffened plates, *Computers and Structures* **8**(1): 51-60.

[5] Sadek E. A., Tawfik S. A., 2000, A finite element model for the analysis of stiffened laminated plates, *Computers and Structures* **75**(4): 369-383.

[6] Liew K. M., Lam K. Y., Chow S. T., 1990, Free vibration analysis of rectangular plates using orthogonal plate function, *Computers and Structures* **34**(1): 79-85.

[7] Aksu G., Ali R., 1976, Free vibration analysis of stiffened plates using finite difference method, *Journal of Sound and Vibration* **48**(1): 15-25.

[8] McBean R., 1968, *Analysis of Stiffened Plates by the Finite Element Method*, Thesis, Stanford University.

[9] Nguyen-Thoi T., Bui-Xuan T., Phung-Van P., Nguyen-Xuan H., Ngo-Thanh P., 2013, Static, free vibration and buckling analyses of stiffened plates by CS-FEM-DSG3 using triangular elements, *Computers and Structures* **125**: 100-113.

[10] Azizian Z., Dawe D., 1985, The analytical strip method of solution for stiffened rectangular plates using finite strip method, *Computers and structures* **21**(3): 423-436.

[11] Mukhopadhyay M., 1989, Vibration and stability of analysis of stiffened plates by semi-analytic finite difference method, Part II: Consideration of bending and axial displacements, *Journal of Sound and Vibration* **130**: 41-53.

[12] Wen P., Aliabadi M., Young A., 2002, Boundary element analysis of shear deformable stiffened plates, *Engineering Analysis with Boundary Elements* **26**(6): 511-520.

[13] Liu G., 2005, *An Introduction to Meshfree Methods and Their Programming*, Springer.

[14] Liu G., 2009, *Mesh Free Methods: Moving Beyond the Finite Element Method*, CRC Press.

[15] Ardestani M. M., Soltani B., Shams S., 2014, Analysis of functionally graded stiffened plates based on FSDT utilizing reproducing kernel particle method, *Composite Structures* **112**: 231-240.

[16] Kansa E. J., 1990, Multiquadrics-a scattered data approximation scheme with applications to computational fluid-dynamics-I, *Computers and Mathematics with Applications* **19**(8): 127-145.

[17] Hardy R. L., 1971, Multiquadric equations of topography and other irregular surfaces, *Journal of Geophysical Research* **78**(8): 1905-1915.

[18] Franke R., 1982, Scattered data interpolation:tests of some methods, *Mathematics of Computation* **38**(157): 181-200.

[19] Fasshauer G., 1997, Solving partial differential equations by collocation with radial basis functions, *Proceedings of the 3rd International Conference on Curves and Surfaces, Surface Fitting and Multiresolution Methods*.

[20] Ferreiraa A. J. M., Batrab R. C., Roquea C. M. C., Qianc L. F., Martins P. A. L. S., 2005, Static analysis of functionally graded plates using third-order shear deformation theory and a meshless method, *Composite Structures* **69**(4): 449-457.

[21] Chang S., 1973, *Analysis of Eccentrically Stiffened Plates*, Thesis, University of Missouri, Columbia.

[22] Deb A., Booton M., 1988, Finite element models for stiffened plates under transverse loading, *Computers and Structures* **28**(3): 361-372.

[23] Biswal K. C., Ghosh A. K., 1994, Finite element analysis for stiffened laminated plates using higher order shear deformation theory, *Computers and Structures* **53**(1): 161-171.